

Design and Analysis of UAV Profile for Agriculture and Surveying Application

Mukesh Raju^{1*}, Theerthamalai Pakkiri², Praveenkumar Marankumar¹, Prashanth Marankumar¹ and Inamul Hasan³

¹Department of Aerospace Engineering, ACS College of Engineering, Bangalore 560074, India

²Department of Aerospace & Aeronautical Engineering, ACS College of Engineering, Bangalore 560074, India

³Department of Aeronautical Engineering, ACS College of Engineering, Bangalore 560074, India

ABSTRACT

This study represents the aerodynamic design of an Unmanned aerial vehicle intended for surveillance or agriculture with a maximum take weight of 125 kg. Weight estimation and constraint analysis were done based on the Mission profile. Design of Computer-Aided Design (CAD) models were generated for three different configurations using CATIA V5R20 as a high wing, mid-wing, and low wing. Flow analysis was done for the above configurations at various angles of attack. ANSYS 15 was used for the flow Analysis. A Tetrahedron element meshed the model with the minimum required orthogonal quality. Five microns were given to the initial layer height of the prism mesh. Spalart Allmaras model is used as the Turbulence model in the solver. The aerodynamic characteristics of the above configuration obtained from Computational Fluid Dynamics (CFD) results were compared with the DATCOM program and validated with the wind tunnel experimental test data. The open-circuited suction-type Subsonic wind tunnel was employed for the test. The aerodynamic properties for the angle of attack in the range of -2° to 14° angle of attack are calculated using a six-component balance.

The study aims to find the Unmanned Aerial Vehicle (UAV) configuration based on the aerodynamic characteristics obtained from the CFD and DATCOM results. High-wing UAVs have better aerodynamic efficiency than the other two configurations.

ARTICLE INFO

Article history:

Received: 27 July 2023

Accepted: 17 October 2023

Published: 19 January 2024

DOI: <https://doi.org/10.47836/pjst.32.S1.01>

E-mail addresses:

vsmprm@gmail.com (Mukesh Raju)

ptmalai@gmail.com (Theerthamalai Pakkiri)

praveenkumarm5195@gmail.com (Praveenkumar Marankumar)

prashanthm1896@gmail.com (Prashanth Marankumar)

aero.inamulhasan@gmail.com (Inamul Hasan)

*Corresponding author

Keywords: Aerodynamic efficiency, CFD analysis, DATCOM, UAV, wind tunnel testing

INTRODUCTION

An unmanned aerial vehicle is an aircraft without a pilot or passengers, generally called a drone. The flight path of UAVs is controlled and operated either with dynamic automation systems or autonomously using preprogrammed flight paths or by remote control from a pilot. Pilot control may be controlled either from the ground or from another vehicle.

Three important parts are required for a UAV to have a successful flight. First is the aerial platform, which contains the navigation system, the airframe, the payload, and the power system. Second is the Ground Control Station (GCS), which helps provide human control remotely. Finally, the communication system helps transfer communication between the ground and the vehicle.

UAVs are nowadays used in various applications. In intelligence and reconnaissance missions, in the operation of stealth-type like micro or mini-UAVs, insect-type small structures, such as flapping-wing ornithopters, make surveillance and targets easy. Also, it is very helpful in aerial photography, LiDAR platforms, and filmmaking in urban and rural areas with less space and in rescue and surveillance activities such as the search for missing persons and firefighting. UAVs are used in many applications where aircraft or helicopters cannot be used due to the size and shape of the vehicle. Some other applications are remote sensing, forest fire, and transportation of goods.

The advantages of UAVs are mainly environmental safety, cost-cutting technology, better quality of aerial photography, programmed precisely to a specific location, easily controllable or deployable, reduced danger and health risks, and flexibility for quick inspections and reaching hazardous areas with easy navigation. Some limitations of UAVs are that they may trespass in an individual private place and fall prey to manipulation. Some restrictions from the government and the local city will make it difficult to fly UAVs in a restricted area, causing legal action. Sometimes, the installed software issues or malfunctions will lead to failure in the respective mission.

The conceptual design of agricultural aircraft optimized for aerodynamic performance is represented by Bravo-Mosquera et al. (2018). The authors designed six configurations by changing the cant angles of the winglet in UAV to obtain the best aerodynamic characteristics through CFD analysis. The overall aerodynamic performance obtained from CFD for the baseline concept with optimal multi-winglet design has been compared. The survey of UAVs used in disaster research and management concept with imagery acquisition was studied by Adams et al. (2013). To improve the performance of UAVs in pressurized structures-based technologies by examining how to construct the UAV with a considerable weight percentage that should be supported by an inflatable structure containing air and concluded that the pressurized structures-based technologies reduce the energy required to keep the UAV aloft (Edge et al., 2010). The procedure for constructing a UAV by Laghari et al. (2023) has designed a UAV that acts as a path glider in normal situations and as a fire

extinguisher in emergencies. The conceptual design of an agricultural aircraft intended for agricultural industry needs was summarized. The proposed design suits the requirements of variable load and low-altitude flight (Sharma & Manna, 2017). The design and aerodynamic performance analysis for a UAV with a payload of 60 kg by increasing the span efficiency. The author compared various wingtip geometries for better performance and an effective aerodynamic improvement by reducing complicated algorithms and time (Turanoguz & Alemdaroglu, 2015).

The optimized design of the drone can be obtained by reducing the weight and maintaining the strength along with reducing the deformation at a higher temperature with the selected AL-7075 T6 for reducing the weight of drone (Hasan et al., 2022a; Khamsi, 2019). The aerodynamic characteristics of Hawkeye UAVs with the help of flow analysis using Reynolds-averaged Navier-Stokes equations for numerical methods and the Spalart-Allmaras Turbulence model are used for simulation. The authors concluded that both the moment and lift co-efficient of Hawkeye UAV were lesser than TERES-02 aircraft due to improper wing design (Johari et al., 2021). The conceptual design of a fixed-wing UAV using a Conventional aircraft design approach and estimated the take-off weight using CFD analysis for optimized design for aerodynamic efficiency by Sharif (2021). The design and analysis of UAV with solar energy as a power source for long endurance at low altitudes concluded that the Solar UAV is an alternative to the conventional UAV for long endurance flight, which can be used for surveillance (Sri et al., 2016).

The design of a trim distributed electric propulsion-based blended wing body configuration by CFD simulation and Wind tunnel testing to evaluate the design quality and obtained the lift-to-drag ratio of 22.31 at an angle of attack of 4° . The cruise condition's pitching moment and static margin met the required design requirements (Wang & Zhou, 2022). The design of agricultural use of unmanned aerial vehicles concluded that the UAVs did not require a separate navigation station and airport since they could be landed on the edge of the agricultural land. UAVs also reduce the no-land flight rate due to lower labor intensity and lower operational costs (del Cerro et al., 2021). The applications of UAV in physiological and biophysical assessments, spraying of phytosanitary, monitoring the biological targets, and topographic surveys were studied by Amaral et al. (2020). The author concluded that the UAV could replace human activities in agriculture, like crop monitoring phytosanitary and spraying pesticides. The usage of UAVs in the agricultural field was studied, and it concluded that UAVs could improve field management and productivity can also be increased. Also, UAVs cannot address every issue in the field, but they can help with some specific agricultural difficulties (Norasma et al., 2019). The preliminary design of UAVs used for surveillance during fire and rescue using CFD concluded that the CFD results match the experimental and real-time conditions (Casas et al., 2008).

The design of UAVs with mathematical models for small UAVs step-by-step used USAF Digital DATCOM to estimate the aerodynamic coefficients. It also concluded that DATCOM offers less precision than CFD and wind tunnel tests, but it operates significantly more effectively by cutting down on significant processing time and design costs. Also, the coefficients of state-space matrices can be calculated using stability and control coefficients and derivatives acquired from DATCOM (Elharouny et al., 2012). The CFD simulation to calculate the unmanned aerial vehicle's (Khau) aerodynamic coefficients using the DATCOM and compared them with the wind tunnel test data proved that the N-S computational method had a better agreement with the test data. However, there is a discrepancy with the DATCOM in the prediction of the moments, but there is a good agreement with the lift coefficient in the DATCOM data (Shafer et al., 2014). The aerodynamic coefficients of unmanned aerial vehicles using Favre-Averaged Navier Stokes in CFD and compared the data with the wind tunnel data using thin and hybrid boundary layer approach to calculate the aerodynamic performance. This study concluded that the thin boundary layer approach has discrepancies in high angles of attack but reduced the computational time.

In contrast, the hybrid boundary layer approach could only increase lift prediction compared to the thin boundary layer approach. Still, it did offer improvements in computational time and convergence of the solution at high angles of attack (Shah et al., 2018). The 3-D simulation for the NACA airfoil and Pioneer RQ-2A piloted vehicle was performed using the three-dimensional, transient, and incompressible formulation for the Reynolds number ranging from 5×10^4 to 2.88×10^6 for different angles of attack and validated with wind tunnel test data. The author concluded that the prediction had a better agreement with the wind tunnel data; the vortex shedding and the streamline and vortex structure highlighted wing tip vortices at high angles of attack (Liu et al., 2020). The procedure for predicting the aerodynamic coefficients for Boeing 747 from the geometrical parameters using the software XFLR and DATCOM was conducted and concluded that the XFLR and DATCOM data had very good longitudinal stability and control data with the derivatives and they are reliable, but XFLR is a better tool than the DATCOM due to some of the inherent limitations in DATCOM (Ahmad et al., 2021).

MATERIALS AND METHODS

The flow of the project starts with mission requirements wherein particular launch altitude, cruise altitude, payload capacity, range, and endurance have been considered. Initial weight estimation has been done. The primary and secondary sub-systems were selected using this initial mass estimation. Considering the initial mass estimation, the initial layout configuration was started, and six types of UAV configurations were designed to satisfy the mission requirement. Then, the selected six design configurations were imported to

the CFD analysis tool for the post-processing work, i.e., calculating lift, drag, and moment coefficients. Then, using the DATCOM program, the co-efficient of lift, drag, and moment were tabulated for the six design configurations. The values obtained from CFD analysis were compared with DATCOM program values to select the UAV configuration with better aerodynamic performance for the mission requirements considered. The flow chart of the research work is shown in Figure 1.

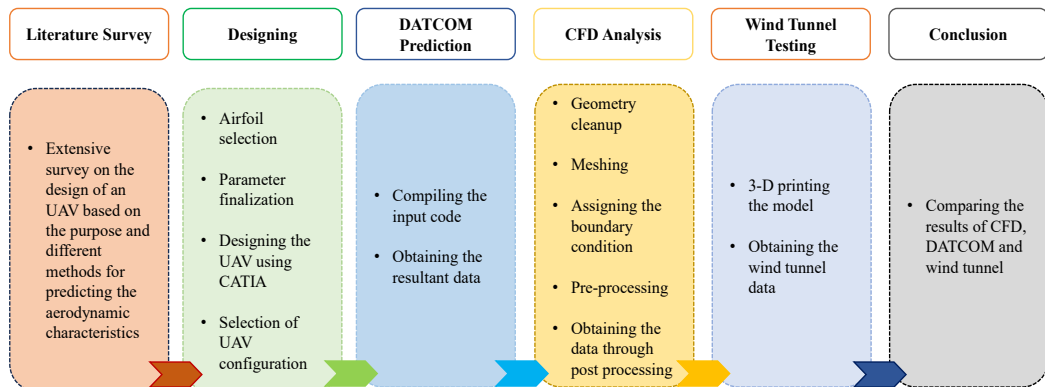


Figure 1. Flowchart of the project

Modeling and Analysis

As mentioned above in the abstract, the design was made using the CATIA V5R20 software. A generative shape design tool was used for designing the UAV components. From the Microsoft Excel file, General Station Description (GSD) Point Spline Loft file was used to generate the airfoil shape with NACA 241-212, NACA 2412, and NACA 0012 using CATIA software for the wing, horizontal, and vertical tail.

The dimension of the fuselage is 3.25 m x 0.3 m, the ogival nose length is 0.6m, boat tail length is 0.3 m. It has been selected for the design and designed per the mentioned dimensions. The aspect ratio value of 5 and taper ratio value of 0.5 were selected for the wing, horizontal, and vertical tail design. The dimensions of the wings have the following data. The wingspan is 2.2678 m, the wing area is 1.0286 m², and the wing incidence angle of 1° has been selected for the design. The dimensions of a horizontal tail have the following data. A span of 0.9328 m and a tail area of 0.1740 m² were selected for the design. The dimensions of the vertical tail are a semi-span of 0.5597 m and a tail area of 0.1740 m² was selected. In generative shape design, the design fuselage revolve option is used after the completion of the sketch. Similarly, multi-section surface and fill options were used for the wing, horizontal, and vertical tail.

UAV Design Layout

Using the above UAV components design, the assembly was made. The assembly design tool was used in CATIA software for the assembly. The offset constraint option was used to assemble all the UAV components in the assembly design tool. The complete UAV assembled section is shown in Figure 2, and the model's detail is shown in Tables 1(a) and 1(b).

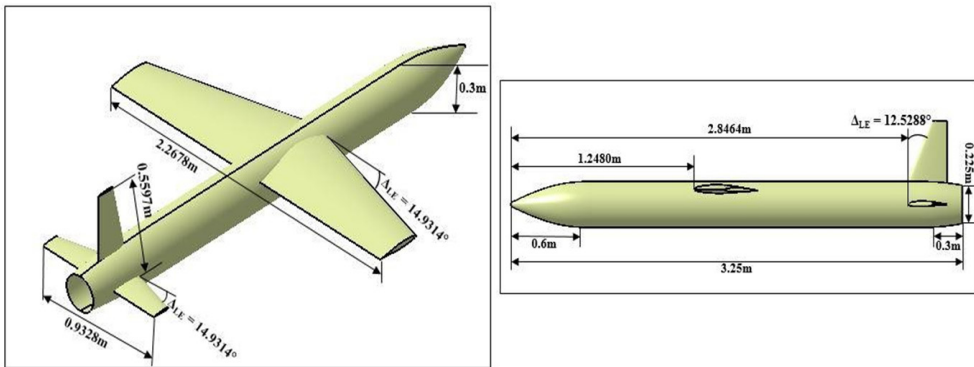


Figure 2. Conventional type-high wing UAV configuration

Table 1(a)
Details of the fuselage

Fuselage Parameter	Dimension
Fuselage Length	3.25 m
Fuselage Diameter	0.3 m
Fuselage Base Diameter	0.225 m
Fuselage Nose Length	0.6 m
Fuselage Base Length	0.3 m

Pre-Processing Work

The ANSYS software was used for pre-processing, including domain creation, application of boundary conditions, meshing, and aerodynamic analysis. Creating domain, meshing, and analysis was done using ANSYS software. The designed model was imported to the ICFM CFD tool in ANSYS software, and the spherical domain was created with a radius of 100m. The imported model and the spherical domain created for the model are shown in Figure 3.

Table 1(b)
Details of the wing, horizontal tail, and vertical tail

Parameters	Wing	Horizontal Tail	Vertical Tail
Airfoil	NACA 641-212	NACA 2412	NACA 0012
Root Chord	0.6047	0.2488	0.2488
Tip Chord	0.3024	0.1244	0.1244
MAC	0.4704	0.1935	0.1935
Leading Edge Sweep	14.93	14.93	12.53
Incidence Angle	1°	-	-
Span	2.2678	0.9328	0.5597
Aspect Ratio	5	5	5
Planform Area	1.0286	0.174	0.174
Leading Edge Position from the Nose	1.248	2.8464	2.8464

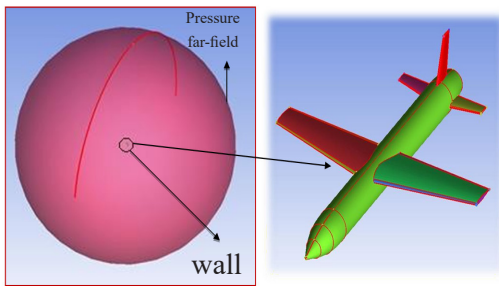


Figure 3. Domain created for the UAV model

The mesh parameters, such as size and type, were selected, and the element size was specified in the setup. Then, the mesh was generated. The robust Octree method was used for creating the surface mesh, and Quick Delaunay was used for creating the volume mesh. A prism layer of 15 numbers was created around the model with an initial height of 5 microns. 91,80,225 elements were generated with 24,58,615 nodes. The

Grid independent study was carried out to get accurate results. The grid-independent study was carried out for 66,92,668 elements, 83,78,783 elements, 87,86,592 elements, 91,80,225 elements, and 1,24,67,408 elements. The results obtained for the third, fourth, and fifth have almost the same aerodynamic coefficient value; hence, the fifth mesh set is selected. Then, the Boundary Condition was assigned to the model and the domain. The surface mesh was generated to the domain, and the details of the mesh parameters are shown in Table 2. Then, the meshed domain and the models are shown in Figure 4.

Table 2
Meshing parameter

Parameter	Specifications
Topology Tolerance	0.1 mm
Element Scale Factor	1
Max. Element Size	10000
Type of Shell Mesh	All-Tri
Meshing Method	Patch-Dependent
Type of Volume Mesh	Mixed/Tetra
Meshing Method	Robust (Octree), Quick Delaunay
Tetra Size Ratio	1.2
Prism Height Limit Factor	0.33
No. Prism Layer	15
Prism Initial Height	4 microns

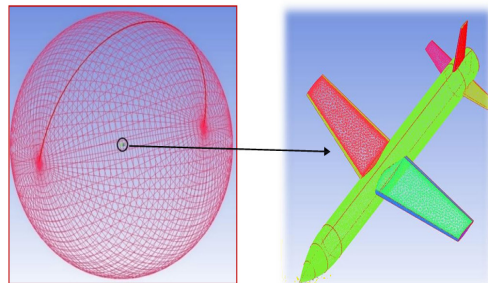


Figure 4. Surface mesh at the model and the domain

After surface meshing, volume mesh was generated to the surface meshed domain and the UAV model. Then, the prism layer was generated on the surface of the UAV. The cross-sectional view of the volume mesh for the domain and the model is shown in Figure 5, the prism layer on the surfaces of the UAV is shown in Figure 6, and the solver parameters are shown in Table 3.

The generated mesh was imported to fluent, and then the SA model and the properties of the air were assigned. The velocity magnitude and direction were given in the boundary condition, and the reference values were given. The analysis was done for the Mach number of 0.31, and the data was saved in the case and data format. The results were post-processed for the analyzed data. Pressure contours and velocity streamlines were taken during post-processing. The CL, CD, and CM data obtained are based on the governing equations mentioned in section 3.2.1, and the data obtained are discussed in the result section.

Table 3
Solver parameters

Parameter	Specifications
Solver Type	Pressure based
Viscous Model	Spalart Allmaras
Energy Equation	On
Density	Ideal Gas
Viscosity	Sutherland
Operating Pressure	0
Gauge Pressure	37601.7 N/m ²
Mach Number	0.31
Temperature	238.619 K
Reference Area	1.0286
Reference Length	0.4074

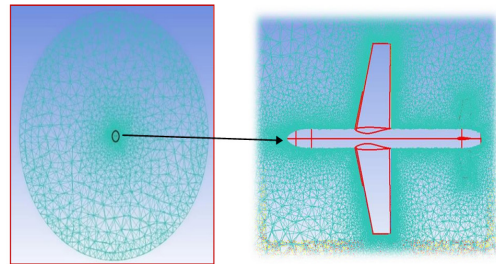


Figure 5. Cross-sectional view of volume mesh

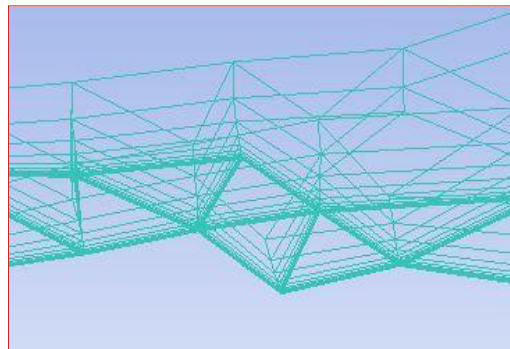


Figure 6. Prism layer on the surface of the UAV

Governing Equations

Basic governing equations are conservation of mass, momentum, and energy under steady-state conditions in 3D form for incompressible and compressible fluid are given below (Hasan et al., 2022b). The fluid that we have used in this study is air. Neglecting the body forces the general form of the continuity, momentum, and energy equations can be written in a Cartesian tensor form as follows:

Continuity Equation. The continuity equation is obtained from conservation laws, which can be derived from Gauss's and Ampere's laws. The concept of mass flow and mass flux is important. Mass can neither be created nor destroyed, and the continuity equation is mentioned in Equation 1.

$$\frac{\partial u}{\partial x} + \frac{\partial v}{\partial x} + \frac{\partial w}{\partial x} = 0 \quad (1)$$

Momentum Equation. Under steady-state conditions and the fluid properties such as density and dynamic viscosity are considered constant, then body force in all directions is negligible. The Navier-Stokes equation is written in x, y, and z components for 3-D flow, which is mentioned in Equations 2, 3, and 4.

X-momentum:

$$U \left[\frac{\partial u}{\partial x} \right] + V \left[\frac{\partial u}{\partial y} \right] + W \left[\frac{\partial u}{\partial z} \right] = -\frac{1}{\rho} \left[\frac{\partial p}{\partial x} \right] + V \left[\frac{\partial^2 u}{\partial x^2} + \frac{\partial^2 u}{\partial y^2} + \frac{\partial^2 u}{\partial z^2} \right] \quad (2)$$

Y-momentum:

$$U \left[\frac{\partial v}{\partial x} \right] + V \left[\frac{\partial v}{\partial y} \right] + W \left[\frac{\partial v}{\partial z} \right] = -\frac{1}{\rho} \left[\frac{\partial p}{\partial y} \right] + V \left[\frac{\partial^2 v}{\partial x^2} + \frac{\partial^2 v}{\partial y^2} + \frac{\partial^2 v}{\partial z^2} \right] \quad (3)$$

Z-momentum:

$$U \left[\frac{\partial w}{\partial x} \right] + V \left[\frac{\partial w}{\partial y} \right] + W \left[\frac{\partial w}{\partial z} \right] = -\frac{1}{\rho} \left[\frac{\partial p}{\partial z} \right] + V \left[\frac{\partial^2 w}{\partial x^2} + \frac{\partial^2 w}{\partial y^2} + \frac{\partial^2 w}{\partial z^2} \right] \quad (4)$$

Energy Equation. For an incompressible fluid, keeping thermal conductivity constant, no viscosity dissipation, and no heat generation under steady-state conditions. Then, the energy equation reduces, as shown in Equation 5.

$$U \frac{\partial T}{\partial x} + V \frac{\partial T}{\partial y} + W \frac{\partial T}{\partial z} = \alpha \left[\frac{\partial^2 T}{\partial x^2} + \frac{\partial^2 T}{\partial y^2} + \frac{\partial^2 T}{\partial z^2} \right] \quad (5)$$

Where, $\alpha = \frac{k}{\rho C_p}$

Flow Contours

After obtaining the results from the analysis, contour plots of pressure, velocity, temperature, and Mach number contours can be obtained from a fluent solver. This research plotted pressure contours, velocity contours, and velocity streamline contours.

Pressure Contours

The pressure contour of the UAV has been plotted for 2° AOA (Figure 7). The maximum and minimum pressure values have been obtained by plotting the contours. The pressure contours of the complete UAV, wing, horizontal and vertical tail are shown in Figures 7(a) to 7(d), respectively.

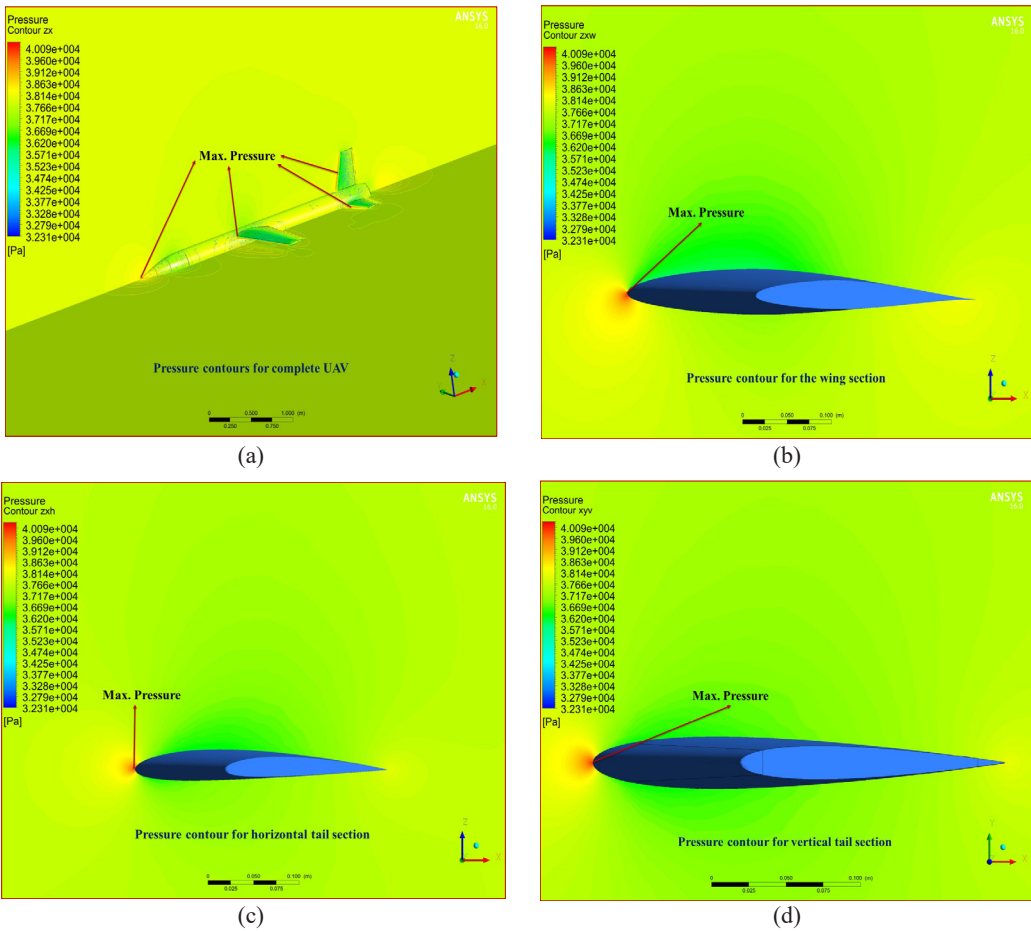


Figure 7. Pressure contours of UAV at 2° AOA (a) Pressure contours for complete UAV (b) Pressure contour for the wing section (c) Pressure contour for horizontal tail section (d) Pressure contour for vertical tail section

Velocity Contours

The velocity contour of the UAV has been plotted for 2° AOA and is shown in Figure 8. The maximum and minimum velocity values have been obtained by plotting the contours. Velocity contours of the complete UAV, wing, horizontal tail, and vertical tail have been shown in Figures 8(a) to 8(d), respectively.

Velocity Streamline Contours

The Velocity Streamline Contour (VSC) of the UAV has been plotted for 2° AOA (Figure 9). Velocity streamline contours represent the fluid flow direction around the UAV's surface. The maximum and minimum velocity streamline values were obtained by plotting the contours. Velocity streamline contours of complete UAV, wing and HT, wing, horizontal tail, and the vertical tail have been shown in Figures 9(a) to 9(e), respectively.

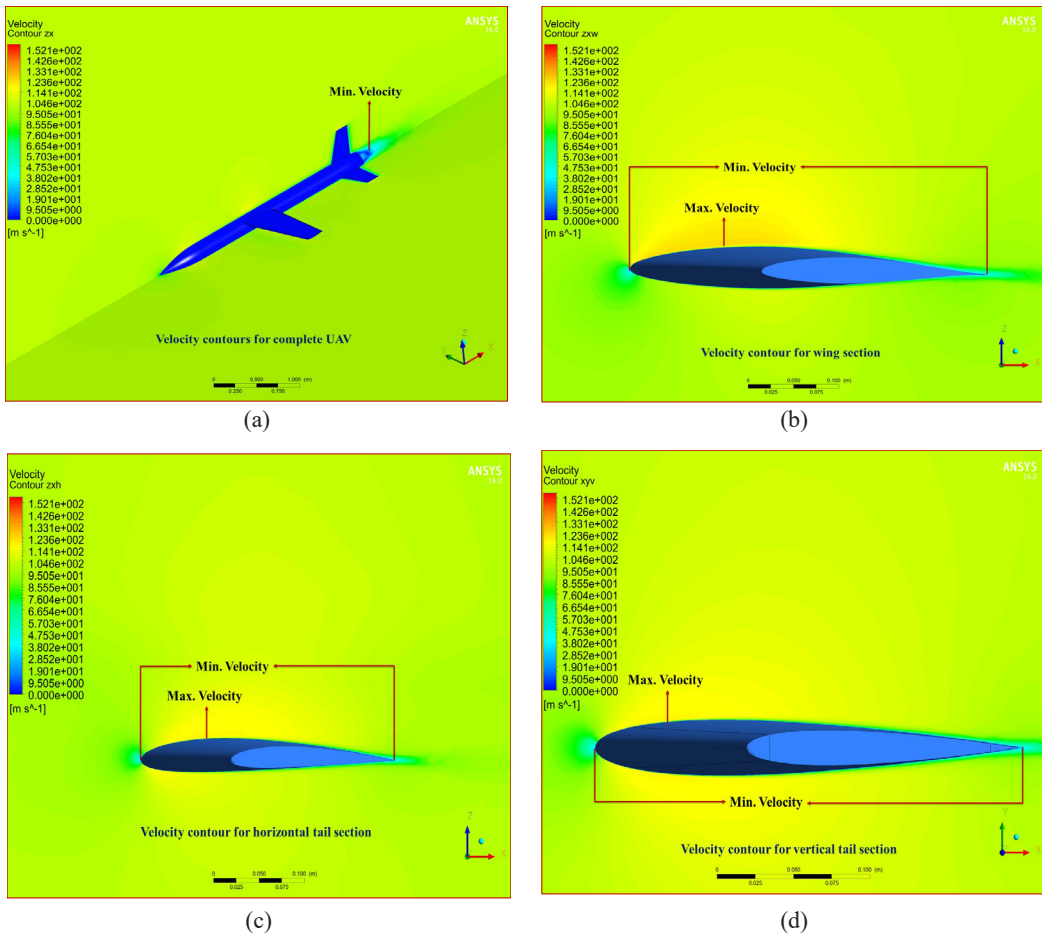
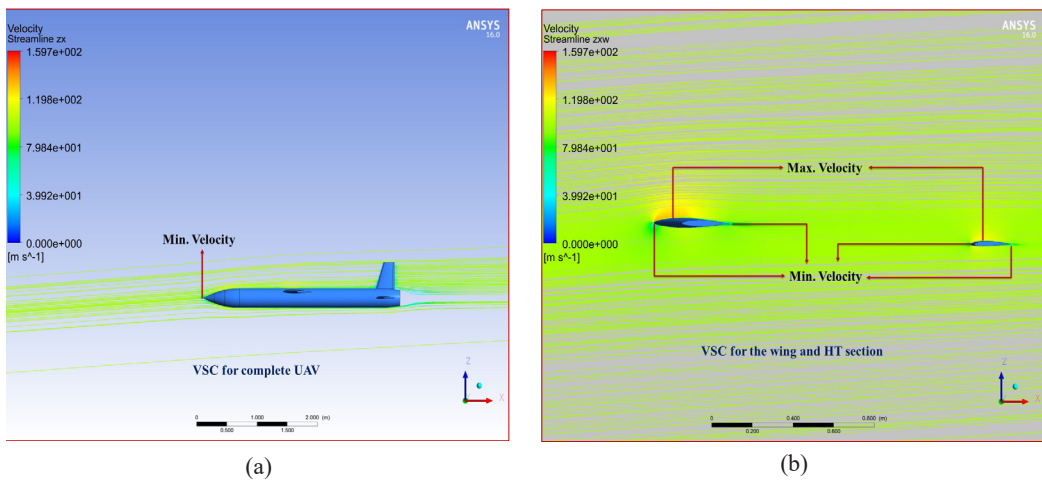
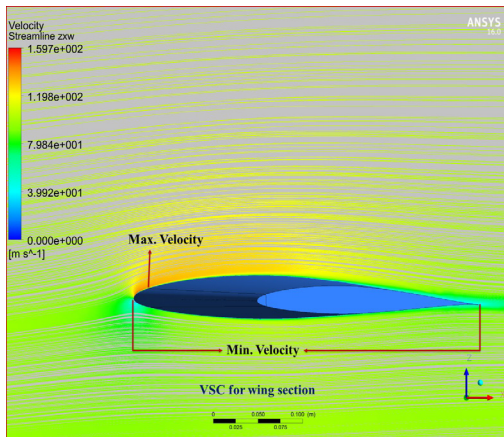
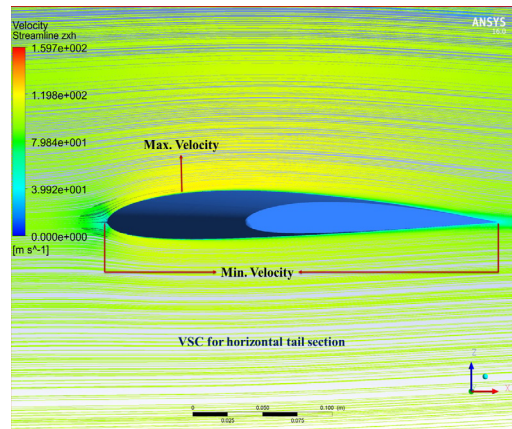


Figure 8. Velocity contours of UAV at 2° AOA (a) Velocity contours for complete UAV (b) Velocity contour for wing section (c) Velocity contour for horizontal tail section (d) Velocity contour for vertical tail section

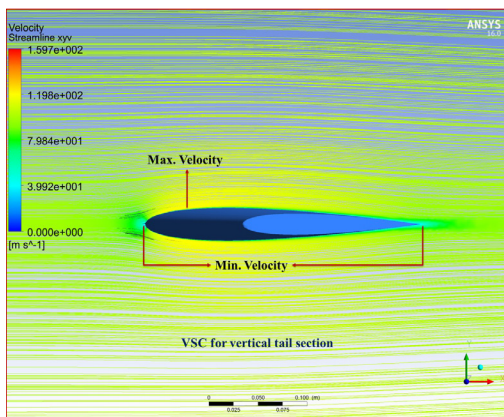




(c)



(d)



(e)

Figure 9. Velocity Streamline contours of UAV at 2° AOA (a) VSC for complete UAV (b) VSC for the wing and HT section (c) VSC for wing section (d) VSC for horizontal tail section (e) VSC for vertical tail section

and is a dimensionless quantity. The moment ratio to the product of dynamic pressure and the wing's surface area is known as the Moment coefficient. The results were obtained for 11 different AOA, i.e., from -6° to 14° with an increment of 2° by changing the X and Y component values in the input values in the software. The values of the coefficient of lift, drag, and moment for different angles of attack are mentioned in Table 1. As per the result mentioned in Table 4, a stall occurs at a 14° AOA, and the maximum lift occurs at a 12° AOA (Piedra et al., 2018; Ramji et al., 2016).

RESULTS AND DISCUSSION

CFD Results

The results are obtained from ANSYS FLUENT by giving the input values like velocity, pressure value, and temperature in the boundary condition. As an output, we get the results like lift coefficient, drag coefficient, and moment coefficient for different angles of attack. The difference between pressure created above and below the body's surface when the body moves around in space and measuring this factor is known as the Lift coefficient. The drag coefficient is used to denote the rearward force that disturbs the airflow of an airfoil

Table 4
CFD result for UAV configuration

SI. No	AOA (α)	C_L	C_D	C_M	C_L / C_D
1	-6°	-0.3287	0.0381	-0.0362	-8.6266
2	-4°	-0.1636	0.0301	-0.0440	-5.4265
3	-2°	0.0028	0.0281	-0.0529	0.1007
4	0°	0.1694	0.0298	-0.0638	5.6886
5	2°	0.3367	0.0353	-0.0798	9.5311
6	4°	0.5057	0.0459	-0.1017	11.0274
7	6°	0.6756	0.0596	-0.1290	11.3299
8	8°	0.8434	0.0777	-0.1595	10.8573
9	10°	1.0074	0.1012	-0.2078	9.9524
10	12°	1.1514	0.1300	-0.2626	8.8557
11	14°	1.0095	0.2311	-0.3826	4.3681

DATCOM Result

The results are obtained from the DATCOM program. In the DATCOM program, some of the parameters of the UAV were given as input values, and input parameters are shown in the Tables 5(a) to 5(e). The parameters like Mach number, Reynolds number, angle of attack, reference area, CG values along the x-axis and z-axis, MAC, the position of the wing, vertical tail, horizontal tail, root chord, tip chord of wing, span, and semi-span of the wing, will be given as inputs and the output file will execute in another file in .out format.

Table 5(a)
General input parameters for the program

General Parameter	Input Values
Mach No	0.31
Alpha sweep	-6° to 14°
Reynolds Number	1.8E+06
Reference Area	1.0286 m ²
Reference Length	0.4074 m
Moment Reference Point	1.5 m

Table 5(b)
Fuselage input parameters for the program

Fuselage Parameter	Input Values
Fuselage Length	3.25 m
Fuselage Diameter	0.3 m
Fuselage Base Diameter	0.225 m
Fuselage Nose Length	0.6 m
Fuselage Base Length	0.3 m

Table 5(c)
Wing input parameters for the program

Wing Parameter	Input Values
Wing Airfoil Type	NACA 641-212
Wingspan	2.316 m
Root Chord	0.617 m
Tip Chord	0.308 m

Table 5(c) (continue)

Wing Parameter	Input Values
Semi Span	1.158 m
Exposed Semi-span	1.009 m
Sweep Angle	14.93°
Wing Incidence Angle	1°
Wing Location from Nose Tip	1.2426 m

Table 5(d)

Horizontal tail input parameters for the program

Horizontal Tail Parameter	Input Values
HT Airfoil Type	NACA 2412
Root Chord	0.1778 m
Tip Chord	0.0889 m
Semi Span	0.3335 m
Exposed Semi-span	0.1864 m
Sweep Angle	14.93°
HT Location from Nose Tip	2.8759 m

Table 5(e)

Vertical tail input parameters for the program

Vertical Tail Parameter	Input Values
VT Airfoil Type	NACA 0012
Root Chord	0.1778 m
Tip Chord	0.0889 m
Semi Span	0.4001 m
Exposed Semi-span	0.2531 m
Sweep Angle	12.53°
VT Location from Nose Tip	2.8759 m

In the output file, the lift coefficient, drag coefficient, pitching moment coefficient, vehicle axial force, vehicle normal force, and side force coefficient will be executed. The results were obtained for the same AOA mentioned in the CFD result. The obtained results are mentioned in Table 6 (Paul et al., 2021; Wu et al., 2019).

Table 6

DATCOM result for UAV configuration

SI. No	AOA (α)	C_L	C_D	C_M	C_L / C_D
1	-6°	-0.3090	0.0370	0.0543	-8.3514
2	-4°	-0.1650	0.0280	0.0151	-5.8929
3	-2°	-0.0280	0.0250	-0.0227	-1.1200
4	0°	0.1070	0.0270	-0.0583	3.9630
5	2°	0.2500	0.0330	-0.0910	7.5758
6	4°	0.4020	0.0460	-0.1218	8.7391
7	6°	0.5610	0.0650	-0.1540	8.6308
8	8°	0.7260	0.0910	-0.1956	7.9780
9	10°	0.8950	0.1250	-0.2384	7.1600
10	12°	1.0680	0.1680	-0.2718	6.3571
11	14°	1.2370	0.2160	-0.3095	5.7296

Wind Tunnel Testing

The wind tunnel model of the UAV was 3D printed utilizing the Fused Deposition Modeling (FDM) method using Polylactic acid (PLA) material with a resolution of 100 microns. To fit inside the wind tunnel test section, the printed model has a scale ratio of 1:6.5, and the 3D-printed UAV model is shown in Figure 10. The experiment was conducted in a subsonic-type wind tunnel with free stream velocities from 5 m/s to 80 m/s and less than 0.5% free stream turbulence intensity. The wind tunnel is shown in Figure 11 and 12 show the model fitted inside the test section. The open-circuited suction type wind tunnel is the type of wind tunnel used for the experimental data analysis. The wind tunnel test section

has the specification of length of 2 m, Width of 0.6 m, and 0.6 m height. Six component balance, the equipment used to determine aerodynamic characteristics, has an AOA range of +20° to -20° for the test trial. The model was tested at 30 m/s while the AOA was changed from -2° to 14°, with a 2° increment in between. The wind tunnel test data obtained are shown in Table 7 (Peng et al., 2022).



Figure 10. Image of the 3D printed model placed in 6 component balance



Figure 11. Image of the wind tunnel



Figure 12. 3D printed model in the test section

Table 7
Experimental results obtained from wind tunnel for the UAV configuration

SI. No	AOA (α)	C_L	C_D	C_M	C_L / C_D
1	-2°	0.2491	0.0623	0.0043	3.9984
2	0°	0.3389	0.0578	-0.0278	5.8633
3	2°	0.3967	0.0630	-0.0662	6.2968
4	4°	0.5168	0.0608	-0.1329	8.5000
5	6°	0.6043	0.0734	-0.1480	8.2330
6	8°	0.6748	0.0927	-0.2047	7.2794
7	10°	0.7534	0.1127	-0.2380	6.6850
8	12°	0.7593	0.2180	-0.2430	3.4830
9	14°	0.7215	0.2358	-0.2094	3.0598

Comparison of DATCOM Values, CFD Values, and Wind Tunnel Experimental Values

The CFD, DATCOM program, and experimental wind tunnel results are compared, like the lift, drag, and pitching moment coefficient. The compared results of CFD, DATCOM, and wind tunnel were plotted in the graphs. Graphs were plotted in four types as a

for C_L/C_D versus angle of attack, which is shown in Figure 16. The values from all three approaches had minor variances when the results were compared. In the coefficient of lift section, stall angles in CFD and experimental results occur at 14° of the angles of attack. However, in DATCOM data, stall angles occur between 16° and 18° of the angle of attack. The calculated values used as input to the program and cause differences in DATCOM results could contain a small proportion of errors.

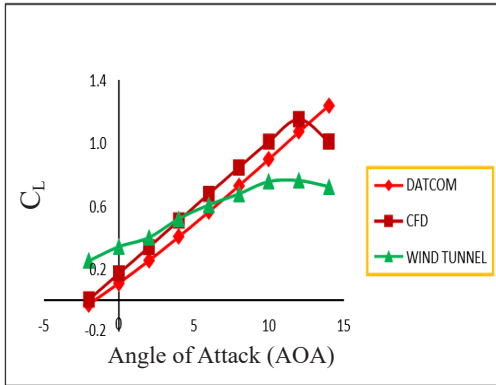


Figure 13. Comparison of DATCOM, CFD, and Wind Tunnel results for C_L vs. AOA

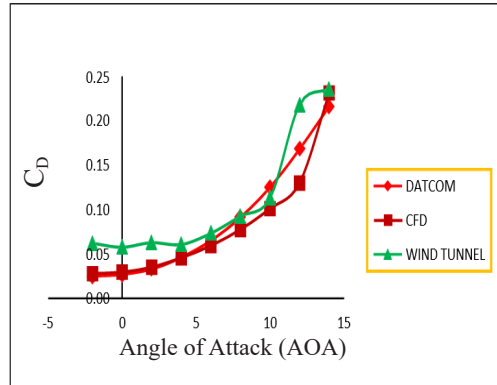


Figure 14. Comparison of DATCOM, CFD, and Wind Tunnel results for C_D vs. AOA

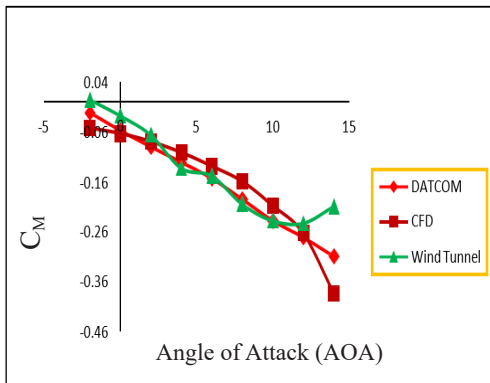


Figure 15. Comparison of DATCOM, CFD, and Wind Tunnel results for C_M vs. AOA

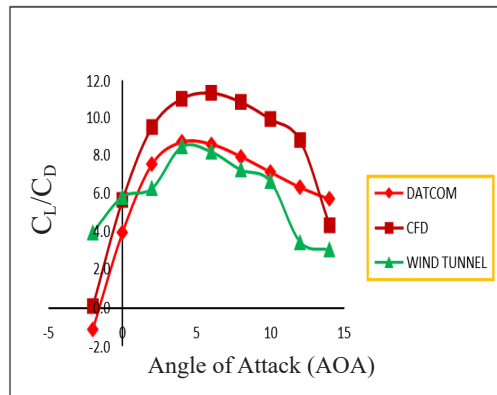


Figure 16. Comparison of DATCOM, CFD, and Wind Tunnel results for C_L / C_D vs. AOA

CONCLUSION

In this work, the aerodynamic performance of a UAV used for agricultural or surveying applications were compared. Initially, three types of UAV configurations were selected. Then, comparing the analysis results, one configuration was selected for better performance. The configurations selected were conventional type-high-wing, conventional type mid-wing, and conventional type low-wing configurations. Analysis was done for different angles of

attack varied from -6° to 14° with an increment of 2° . The aerodynamic performance values like the coefficient of lift, coefficient of drag, and pitching moment coefficient for all three types of configurations were noted down.

Input values were given to the DATCOM program to verify that the obtained CFD result was correct. Once the results from the DATCOM program were obtained, both results were compared. The compared results varied by $\pm 2.8\%$. Then, tests in a wind tunnel were conducted for validation. The experimental data from wind tunnel testing has more closely aligned values, and wind tunnel data agreed well with the CFD and DATCOM results.

Then, from the CFD, DATCOM, and wind tunnel test result data, we can conclude that the conventional type-high wing configuration has better efficiency than the other two configurations. So, the conventional type-high-wing UAV configuration from the design suggested in this research can be used for agricultural or surveying purposes.

ACKNOWLEDGEMENT

The Part of this work is funded by Aeronautical Development Establishment (Defence Research & Development Organization), Bangalore, India. Project grant No: ADE/PPA/14923/CARS/21-22/01.

REFERENCES

- Adams, S. M., Levitan, M. L., & Friedland, C. J. (2013). High resolution imagery collection utilizing unmanned aerial vehicles (UAVs) for post-disaster studies. *Advances in Hurricane Engineering* (pp. 777-793). <https://doi.org/10.1061/9780784412626.067>
- Ahmad, M., Hussain, Z. L., Shah, S. I. A., & Shams, T. A. (2021). Estimation of stability parameters for wide body aircraft using computational techniques. *Applied Sciences*, *11*(5), 2087. <https://doi.org/10.3390/app11052087>
- Amaral, L. R. D., Zerbato, C., Freitas, R. G. D., Barbosa Júnior, M. R., & Simões, I. O. P. D. S. (2020). UAV applications in Agriculture 4.0. *Revista Ciência Agronômica*, *51*(5). <https://doi.org/10.5935/1806-6690.20200091>
- Bravo-Mosquera, P. D., Cerón-Muñoz, H. D., Díaz-Vázquez, G., & Catalano, F. M. (2018). Conceptual design and CFD analysis of a new prototype of agricultural aircraft. *Aerospace Science and Technology*, *80*, 156–176. <https://doi.org/10.1016/j.ast.2018.07.014>
- Casas, L. E., Hall, J. M., Montgomery, S. A., Patel, H. G., Samra, S. S., Si Tou, J., Quijano, O., Mourtos, N. J., & Papadopoulos, P. P. (2008). Preliminary design and CFD analysis of a fire surveillance unmanned aerial vehicle. In *Proceedings, Thermal-Fluids Analysis Workshop* (p. 50).
- del Cerro, J., Cruz Ulloa, C., Barrientos, A., & de León Rivas, J. (2021). Unmanned aerial vehicles in Agriculture: A survey. *Agronomy*, *11*(2), 203. <https://doi.org/10.3390/agronomy11020203>
- Edge, H., Collins, J., Brown, A., Coatney, M., Roget, B., Slegers, N., & Johnson, A. (2010). Lighter-than-air and Pressurized structures technology for Unmanned Aerial Vehicles (UAVs). *Army Research Laboratory Report ARL-TR-5068, Defense Technical Information Center, Army Research Laboratory, Aberdeen Proving Ground, MD, USA*. <https://doi.org/10.21236/ada513823>

- Elharouny, A. S., Youssef, A. M., Zakaria, M. Y., & Abdel-Hameed, M. M. (2012, May). Procedures for mathematical modeling of small unmanned aerial vehicles. In *The International Conference on Applied Mechanics and Mechanical Engineering* (Vol. 15, pp. 1-12). Military Technical College.
- Hasan, I., Mukesh, R., Krishnan, P. R., Srinath, R., Babu, D. P., & Gurmur, N. L. (2022). Wind tunnel testing and validation of helicopter rotor blades using additive manufacturing. *Advances in Materials Science and Engineering*, 2022, 1–13. <https://doi.org/10.1155/2022/4052208>
- Hasan, I., Mukesh, R., Radha Krishnan, P., Srinath, R., & B. Dhanya Prakash, R. (2022). Forward flight performance analysis of supercritical airfoil in helicopter main rotor. *Intelligent Automation & Soft Computing*, 33(1), 567–584. <https://doi.org/10.32604/iasc.2022.023252>
- Johari, M. S., Ali, Z. M., Wisnoe, W., Ismail, N., & Ishak, I. S. (2021). Computational aerodynamic analysis of UiTM's hawkeye UAV aircraft, *Journal of Aeronautics, Astronautics and Aviation*, 53(2), 295-302. [https://doi.org/10.6125/JoAAA.202106_53\(2\).23](https://doi.org/10.6125/JoAAA.202106_53(2).23)
- Khamisi, M. (2019). Design and analysis of an unmanned aerial vehicle capable of carrying the camera. *Universal Journal of Mechanical Engineering*, 7(3), 87–96. <https://doi.org/10.13189/ujme.2019.070302>
- Laghari, A. A., Jumani, A. K., Laghari, R. A., & Nawaz, H. (2023). Unmanned aerial vehicles: A review. *Cognitive Robotics*, 3, 8–22. <https://doi.org/10.1016/j.cogr.2022.12.004>
- Liu, I.-H., Torelli, R., Prabhakar, N., & Karbowski, D. (2020). CFD modeling of unmanned aerial systems with cut-cell grids and adaptive mesh refinement. In *AIAA Scitech 2020 Forum* (p. 0538). <https://doi.org/10.2514/6.2020-0538>
- Norasma, C. Y. N., Fadzilah, M. A., Roslin, N. A., Zanariah, Z. W. N., Tarmidi, Z., & Candra, F. S. (2019). Unmanned aerial vehicle applications in agriculture. In *IOP Conference Series: Materials Science and Engineering* (Vol. 506, p. 012063). IOP Publishing. <https://doi.org/10.1088/1757-899x/506/1/012063>
- Paul, J. L., Vasile, J. D., & DeSpirito, J. (2021). Comparison of aeroprediction methods for guided munitions. In *AIAA Scitech 2021 Forum* (p. 0024). <https://doi.org/10.2514/6.2021-0024>
- Peng, X., Zhu, H., Xu, D., Xiao, M., Wang, W., & Cai, G. (2022). Aerodynamic performance uncertainty analysis and optimization of a conventional axisymmetric vehicle based on parallel polynomial chaos expansions. *Aerospace*, 9(8), 396. <https://doi.org/10.3390/aerospace9080396>
- Piedra, S., Martinez, E., Escalante-Velazquez, C. A., & Jimenez, S. M. A. (2018). Computational aerodynamics analysis of a light sport aircraft: Compliance study for stall speed and longitudinal stability certification requirements. *Aerospace Science and Technology*, 82–83, 234–242. <https://doi.org/10.1016/j.ast.2018.09.016>
- Ramji, V., Mukesh, R., & Hasan, I. (2016). Design and numerical simulation of convergent divergent nozzle. *Applied Mechanics and Materials*, 852, 617–624. <https://doi.org/10.4028/www.scientific.net/amm.852.617>
- Shafer, T., Viken, S., Favaregh, N. M., Zeune, C. H., Williams, N., & Dansie, J. (2014). Comparison of computational approaches for rapid aerodynamic assessment of small UAVs. In *52nd Aerospace Sciences Meeting* (p. 0039). AIAA. <https://doi.org/10.2514/6.2014-0039>
- Shah, H., Pampala, R. B., & Olivares, G. (2018). CFD analysis and experimental validation of an unmanned aerial vehicle. In *2018 Applied Aerodynamics Conference*. AIAA. <https://doi.org/10.2514/6.2018-4216>
- Sharma, N. & Manna, K. T. (2017), Conceptual design approach of agricultural aircrafts. In *International Conference Proceeding ICCCT* (pp. 122-133). IJCRT.

- Sharif, A. (2021). Conceptual design and analysis of a fixed wing mini unmanned aerial vehicle for humanitarian assistance operations. In *AIAA SCITECH 2022 Forum* (p. 1504). <https://doi.org/10.2514/6.2022-1504>
- Sri, K. R. B., Aneesh, P., Bhanu, K., & Natarajan, M. (2016). Design Analysis of solar-powered unmanned aerial vehicle. *Journal of Aerospace Technology and Management*, 8(4), 397–407. <https://doi.org/10.5028/jatm.v8i4.666>
- Turanoguz, E. & Alemdaroglu, N. (2015, June, 9-12). Design of a medium range tactical UAV and improvement of its performance by using Winglets. In *2015 International Conference on Unmanned Aircraft Systems (ICUAS)* (pp. 1074-1083). IEEE. <http://doi.org/10.1109/ICUAS.2015.7152399>
- Wang, K., & Zhou, Z. (2022). Aerodynamic design, analysis and validation of a small blended-wing-body unmanned aerial vehicle. *Aerospace*, 9(1), 36. <https://doi.org/10.3390/aerospace9010036>
- Wu, H., Gao, M., Song, W., Jie, Z., & Wang, Y. (2019). Accuracy analysis of aerodynamic calculation of twodimensional ballistic correction projectile based on missile datcom. *IOP Conference Series: Materials Science and Engineering*, 612(3), 032096. <https://doi.org/10.1088/1757-899x/612/3/032096>

